IEEE Access
Multidisciplinary ⋮ Rapid Review ⋮ Open Access Journal

Received 15 August 2025, accepted 25 August 2025, date of publication 8 September 2025, date of current version 1 October 2025.

Digital Object Identifier 10.1109/ACCESS.2025.3606978

RESEARCH ARTICLE

Aerial Reconfigurable Intelligent Surface Assisted Vehicle-to-Vehicle Communication

NORLEZAH HASHIM[1], (Graduate Student Member, IEEE),
CHEE YEN LEOW[1], (Senior Member, IEEE),
KLAUS MOESSNER[2], (Senior Member, IEEE),
AND CHUAN HENG FOH[3], (Senior Member, IEEE)

[1]Wireless Communication Centre, Faculty of Electrical Engineering, Universiti Teknologi Malaysia, Skudai, Johor 81310, Malaysia
[2]Department of Communications Engineering, TU Chemnitz, 09111 Chemnitz, Germany
[3]5G/6G Innovation Centre, Institute for Communication Systems, University of Surrey, GU2 7XH Guildford, U.K.

Corresponding author: Chee Yen Leow (bruceleow@utm.my)

This work was supported by the Horizon 2020 Marie Skłodowska-Curie Actions Research and Innovation Staff Exchange (H2020-MSCA-RISE-2020) Project SwiftV2X under Grant Agreement No. 101008085, and in part by the Ministry of Higher Education Malaysia through the Higher Institution Centre of Excellence (HICOE) under Grant 4J636.

ABSTRACT Vehicle-to-vehicle (V2V) communication enhances safety by allowing moving vehicles to exchange real-time information. However, due to dynamic environments, V2V links are vulnerable to blockage due to obstacles. We propose the use of aerial reconfigurable intelligent surface (ARIS) mounted on an unmanned aerial vehicle (UAV) to enhance V2V communication reliability by reflecting the signal between moving vehicles. Then we adopt the power consumption models for multirotor UAVs, where three flight statuses, i.e., forward flight, vertical ascent, and vertical descent, are included into the system model. The optimization problem is formulated to maximize energy efficiency (EE) by jointly optimizing the three-dimensional (3D) position of ARIS and the transmit power of the system, while ensuring a minimum data rate requirement to meet quality-of-service (QoS) constraints. Due to the non-convexity of the formulated problem, the EE optimization is solved using Dinkelbach's iterative algorithm and interior point method. Simulation results demonstrate that the proposed scheme outperforms benchmark methods, with optimized hybrid ARIS yielding the highest EE compared to passive ARIS scheme.

INDEX TERMS Energy efficiency, ARIS, 3D position, transmit power, V2V communication.

I. INTRODUCTION

Vehicle-to-Everything (V2X) technology has the potential to enhance transportation safety and efficiency, eventually unlocking the full potential of connected and autonomous vehicles (CAVs). Vehicle-to-vehicle (V2V) communication enhances the safety by allowing CAVs to exchange real-time information including time-sensitive data from vehicle sensors, which is crucial in mission-critical and emergency applications. However, due to the dynamic vehicular environment, the links can be blocked by obstacles which hinder the direct line-of-sight (LoS) communication between vehicles [1]. A potential solution is by introducing reconfigurable intelligent surface (RIS), a planar metasurface composed of numerous reflecting elements. Each element can independently control the phase shift and amplitude of the incident signal, allowing it to be reflected toward a desired receiver [2]. Recent studies have demonstrated the effectiveness of RIS in vehicular environments, where LoS links often get disrupted by high mobility and dynamic obstacles. The authors in [3] proposed transmission protocols and resource allocation strategies to reduce signaling overhead and mitigate channel ageing. Similarly, [4] emphasizes the role of meta-surfaces in supporting the development of low-latency and energy-efficient vehicular networks.

Previous works proposed terrestrial RIS (TRIS) by placing them on the building or along the road [2], [5]. TRIS offers limited coverage, which poses a challenge for V2V cases.

The associate editor coordinating the review of this manuscript and approving it for publication was Olutayo O. Oyerinde.

To support a long stretch of road, multiple TRIS units are required, along with frequent switching between RIS panels to maintain continuous connectivity [6]. Thus, TRIS might not be efficient for V2V applications. Alternatively, aerial RIS (ARIS) can be employed, where RIS is mounted on an unmanned aerial vehicle (UAV) that follows the vehicles to maintain a stable V2V link. The authors in [7] conducted a preliminary case study to evaluate the potential of ARIS for V2V and vehicle-to-infrastructure (V2I) in fifth-generation (5G). They show ARIS offers advantages in maximizing the achievable rate compared to TRIS.

Up to now, there has been limited literature on ARIS within V2V context. In [8], a trajectory model was proposed to ensure LoS communication links for a millimetre Wave emergency vehicle. A two-stage method is proposed; in the first stage, the optimal tube path is determined by considering energy consumption, UAV speed constraints, and the LoS link using dynamic programming. In stage two, the optimal ARIS trajectory is determined, and simulation results show the improvement in terms of energy efficiency and LoS-secured path of ARIS. The work is extended in [9] by adding a group of ARISs to sustain reliable LoS links with a group of ground vehicles. Taking into account energy efficiency, constraints, and channel gains, a consensus-based coordinating strategy is employed to make sure all ARISs provide coverage to all the targetted ground vehicles. Research works in [8] and [9] focused on fixed ARIS altitude and UAV-to-vehicle (U2V) link, where from results obtained earlier in [10], a broader margin of rate is observed when the altitude of ARIS is optimized as it improves the LoS due to fewer obstacles observed and better elevation angle.

Additionally, all of the previously listed researches consider passive ARIS [2], [5], [6], [7], [8], [9], where the passive reflecting gains are limited and degrade with increasing distance between the transmitter and receiver due to the absence of amplification to sustain the channel gains. Besides, the passive scheme often suffers a double path-loss effect, especially when ARIS is far from the transmitter or receiver [11]. The use of hybrid RIS has demonstrated improvement compared to passive RIS [12]. Hybrid RIS overcome the limitations of passive RIS, by simultaneously enabling both reflection and amplification gains. This is achieved through the integration of reflection-type amplifiers with a small number of active elements. Compared to fully active ARIS, hybrid ARIS is the preferred method due to lower hardware cost and minimal power consumption. However, to the author's knowledge, the study on hybrid ARIS for V2V communication is still an open problem.

The proposed ARIS-aided V2V system is particularly applicable in practical vehicular environments where communication links are frequently obstructed by large vehicles or urban infrastructure and where base station (BS) or access point (AP) coverage may be limited or entirely unavailable. For example, in urban highways with LoS blockage, UAV-mounted RIS can dynamically restore and enhance the V2V link without relying on fixed infrastructure. The system can be deployed in emergencies or temporary communication setups. This makes it highly suitable for future intelligent transportation systems, especially in disrupted environments or disasters [13]. Therefore, in this work, we propose a hybrid ARIS for V2V communication systems and formulate an optimization problem aimed at maximizing the system's energy efficiency (EE). Motivated by the above concerns:

1) We consider a V2V communication scenario where the base station is not accessible due to reasons such as extreme path loss, severe blockage or malfunctioning and communication is established using ARIS. Vehicle receives data from another vehicle, and due to obstacles, there is no or a weak direct link between them. We propose to maximize the EE of ARIS to establish and maintain a V2V communication. The optimization problem is formulated as a function of transmit power and three-dimensional (3D) position of ARIS while a practical energy model for multi-rotor UAV is implemented, which includes three types of flight energy: horizontal flight, vertical ascent and descent flight of UAV.

2)The formulated optimization problem is fractional and non-convex. To solve it, we employ the Dinkelbach iterative algorithm in conjunction with the interior-point method.

3) Simulation results demonstrate that hybrid ARIS scheme achieves superior EE compared with other schemes.

The remainder of this paper is organized as follows. Section II presents the system model and problem formulation. In Section III, the proposed algorithms are explained in detail, and Section IV provides the simulation results and performance evaluation of the proposed algorithm. Finally, the paper is concluded in Section V.

II. SYSTEM MODEL

We consider an ARIS assisted V2V communication, which consists of a vehicle source V_1, a vehicle user V_2, a RIS mounted on a rotary-wing UAV as in Fig. 1. It is assumed that the direct link from V_1 to V_2 is blocked by obstacles and ARIS is used to set up virtual LoS link to the vehicles by reflecting the signal from V_1 towards V_2. A single antenna is used for V_1 and V_2 respectively, while the RIS comprises of N reflective elements. A 3D Cartesian coordinate system is assumed, where the coordinates of the V_1, V_2, and ARIS can be indicated as $(x_{v_1}, 0, 0)$, $(x_{v_2}, , 0, 0)$ and (x_a, y_a, z_a), respectively. Both vehicles and ARIS are moving at different velocity, α_{v1}, α_{v2}, and α_{ARIS}, causing the relative distance between vehicles to increase as a function of time. This study considers a single V2V communication link assisted by an ARIS to establish the baseline system behavior. However, the system model can be extended to multiple V2V pairs, each supported by individual ARIS systems operating over distinct channel resources (e.g., time slots or orthogonal frequencies). These groups can function independently without interference, making the proposed design applicable to scalable vehicular networks [14].

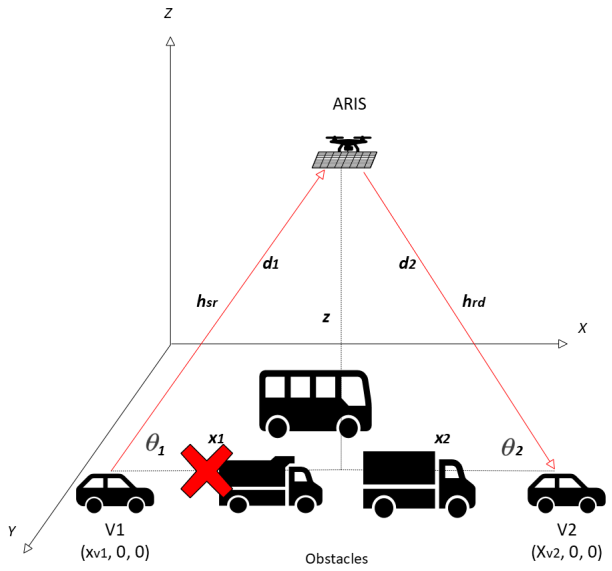

FIGURE 1. ARIS-assisted V2V communication in the presence of obstacles.

A. CHANNEL MODEL

In this setup, we have an ARIS with N discrete elements. The channel from V_1 to ARIS is denoted by $\mathbf{h}_{\text{sr}} \in \mathbb{C}^N$, where $[\mathbf{h}_{\text{sr}}]_n$ denotes the n-th component. The channel between ARIS to V_2 is denoted by $\mathbf{h}_{\text{rd}} \in \mathbb{C}^N$. We assume that the size of each element is smaller than the wavelength, thus it scatters the incoming signal with approximately constant gain in all directions of interest. The channel gain from V_1 to ARIS and from ARIS to V_2 can be defined respectively as [15]:

$$|\mathbf{h}_{\text{sr, rd}}| = A\frac{|\mathbf{\Omega}_{\text{sr, rd}}|^2}{d_j^{\alpha_{\text{sr, rd}}}}. \tag{1}$$

where Ω_{sr} and Ω_{rd} are the random variables, which follow a Rician distribution, independent and identically distributed (i.i.d). Variable A is the constant coefficient, d_j is the Euclidean distance between vehicle and ARIS where $j = 1, 2$. The variables α_{sr} and α_{rd} are the aerial path loss exponents which are described as:

$$\alpha_{\text{sr,rd}} = \alpha_e \text{PNLoS}_{\text{sr,rd}}(\theta) + \alpha_o. \tag{2}$$

where α_e and α_o are the constant values. Using Al-Hourani's channel model [16], the probabilities of LoS (PLoS) and non-LoS (PNLoS) are calculated as:

$$\text{PLoS}_{\text{sr,rd}}(\theta) = \frac{1}{1 + a\exp\left(-b[\theta_j - a]\right)} \tag{3}$$

and

$$\text{PNLoS}_{\text{sr,rd}}(\theta) = 1 - \text{PLoS}_{\text{sr,rd}}(\theta). \tag{4}$$

where a and b are the environmental constants. It is assumed that each channel subjects to block fading and are mutually independent, while the transmitter possesses knowledge of the channel state information (CSI). The coordinates of each vehicle with respect to ARIS are given by x_j and y_j, while z represents the altitude of ARIS. The Euclidean distance between ARIS and each vehicle is then calculated as:

$$d_j = \sqrt{|x_j - y_j|^2 + z^2},\ j \in \{1, 2\}. \tag{5}$$

The elevation angle of ARIS for each vehicle is defined as:

$$\theta_j = \arctan\left(\frac{z}{x_j - y_j}\right), \quad j \in \{1, 2\}. \tag{6}$$

B. TRANSMISSION SCHEME

A) PROPOSED HYBRID ARIS

Several transmission schemes are investigated in this section, including the proposed hybrid ARIS, existing passive ARIS and existing half-duplex relay. Hybrid ARIS consists of N discrete elements, including L active and $N - L$ passive reflecting elements. The signal received at V_2 after reflection from hybrid ARIS is given by [11]:

$$y_h = \sqrt{P_h}\mathbf{h}_{\text{rd}}^H\mathbf{\Phi}_h\mathbf{h}_{\text{sr}}s + \sqrt{P_h}\mathbf{h}_{\text{rd}}^H\mathbf{\Psi}_h\mathbf{h}_{\text{sr}}s + \mathbf{h}_{\text{rd}}^H\mathbf{\Psi}_h n_r + n. \tag{7}$$

where P_h denotes the transmit power of V_1, $n_r \sim CN(0, \sigma_r^2 I_N)$ and $n \sim CN(0, \sigma^2)$ represent the thermal noise at the active elements and V_2, respectively. The matrices $\mathbf{\Phi}_h$ and $\mathbf{\Psi}_h$ represent the reflective coefficients of passive and active RIS elements, respectively, defined as $\mathbf{\Phi}_h = \text{diag}\left\{\Phi_{1,\ldots,}\Phi_N\right\}$ and $\mathbf{\Psi}_h = \text{diag}\left\{\Psi_{1,\ldots,}\Psi_N\right\}$.

$$\mathbf{\Phi}_n = \begin{cases} 0, & n \in \mathbb{L} \\ e^{j\theta_N}, & \text{otherwise} \end{cases}, \tag{8}$$

$$\mathbf{\Psi}_n = \begin{cases} \rho_n e^{j\theta_N}, & n \in \mathbb{L} \\ 0, & \text{otherwise} \end{cases}. \tag{9}$$

The sets $\mathbb{L} \subset \{1, 2, \ldots, N\}$ represent the indices of the active RIS elements. It is assumed that all $\rho_n = \rho$, which means all active elements are identical, then the amplification gain, ρ^2 can be calculated as:

$$\rho^2 = \frac{P_{\text{ris}}}{L\left(P_h|\,\mathbf{h}_{\text{sr}}\,|^2 + \sigma_r^2\right)}. \tag{10}$$

where P_{ris} denotes the transmit power of hybrid ARIS and the equation for P_{ris} can be stated as:

$$P_{\text{ris}} = P_h\,\|\,\mathbf{\Psi}_h\mathbf{h}_{\text{sr}}\,\|^2 + \sigma_r^2\,\|\,\mathbf{\Psi}_h\,\|^2. \tag{11}$$

Thus, the SNR of the hybrid ARIS can be written as:

$$\gamma_{\text{hyb}} = \frac{P_h\left((N-L)^2\,|\,\mathbf{h}_{\text{sr}}\,|^2|\,\mathbf{h}_{\text{rd}}\,|^2 + \rho^2L^2\,|\,\mathbf{h}_{\text{sr}}\,|^2|\,\mathbf{h}_{\text{rd}}\,|^2\right)}{\rho^2\sigma_r^2L\,|\,\mathbf{h}_{\text{rd}}\,|^2 + \sigma^2}. \tag{12}$$

The achievable rate and transmit power of hybrid ARIS scheme can be calculated as [11] and [17]:

$$R_{\text{hyb}} = B\log_2\left(1 + \gamma_{\text{hyb}}\right) \tag{13}$$

and

$$P_h + P_{\text{ris}} = P_{\text{tot}} - NP_{\text{sw}} - LP_{\text{dc}} - P_s - P_d. \tag{14}$$

where B represents the system bandwidth, P_{sw} represents the power consumed by the control circuitry and phase-shift

switch at RIS elements, and P_{tot} is the total power consumption of the system. The terms P_s and P_d account for hardware dissipation power at the source and destination, respectively. Additional power, P_{dc}, denotes the power required for direct current (DC) biasing at each active RIS element in hybrid ARIS.

B) PASSIVE ARIS

In the passive ARIS system consisting of N passive elements mounted on UAV, ARIS reflects the incident signals without any amplification. The reflection matrix of the RIS is defined as $\Phi = \text{diag}\left\{\rho_n e^{j\Phi_1}, \ldots, \rho_n e^{j\Phi_N}\right\}$, where ρ_n is the amplification factor and Φ_n is the phase shift of the n-th RIS reflecting element, with $\Phi_n \in [0, 2\pi)$. For passive RIS, $\rho_n = 1$ which means no signal amplification occurs. Thus, the received signals at V_2 are summarized as [11]:

$$y_p = \sqrt{P_p}\,\mathbf{h}_{\text{rd}}^H \mathbf{\Phi} \mathbf{h}_{\text{sr}}\, s + n. \tag{15}$$

where P_p denotes the transmit power of V_1 in passive ARIS system. It is assumed that the phase shift is ideal, allowing all reflected signals to arrive in phase at V_2. Thus, $\Phi = \Phi_{\text{sr}} + \Phi_{\text{rd}}$ where Φ_{sr} and Φ_{rd} represent the reflection components influenced by the V_1-to-RIS and RIS-to-V_2, respectively. Based on this, the signal-to-noise ratio (SNR) and achievable rate of the passive ARIS system can be expressed as:

$$\gamma_{\text{pas}} = \frac{N^2 P_p \mid \mathbf{h}_{\text{sr}} \mid^2 \mid \mathbf{h}_{\text{rd}} \mid^2}{\sigma^2} \tag{16}$$

and

$$R_{\text{pas}} = B \log_2 \left(1 + \gamma_{\text{pas}}\right) . \tag{17}$$

The total power consumption of passive RIS system is given by [18]:

$$P_p = P_{\text{tot}} - NP_{\text{sw}} - P_s - P_d. \tag{18}$$

C) BASELINE AERIAL RELAY SCHEME

For benchmarking, we also compare with non-ARIS scheme which is half-duplex (HD) UAV relay scheme, it refers to a mode where data transmission can occur in both directions, but not simultaneously. The SNR and achievable rates for both HD schemes, namely decode and forward (DF) and amplify and forward (AF) are given respectively in [11]:

DF SNR and achievable rate:

$$\gamma_{\text{hddf}} = \min\left\{\frac{P_{\text{hd}} \mid \mathbf{h}_{\text{sr}} \mid^2}{\sigma_r^2}, \frac{P_{\text{hdrel}} \mid \mathbf{h}_{\text{rd}} \mid^2}{\sigma^2}\right\} \tag{19}$$

and

$$R_{\text{hddf}} = B \log_2 \left(1 + \gamma_{\text{hddf}}\right) . \tag{20}$$

AF SNR and achievable rate:

$$\gamma_{\text{hdaf}} = \left\{\frac{P_{\text{hd}} \mid \mathbf{h}_{\text{sr}} \beta_h \mathbf{h}_{\text{rd}} \mid^2}{\mid \beta_h \mathbf{h}_{\text{sr}} \mid^2 \sigma_r^2 + \sigma^2}\right\} \tag{21}$$

and

$$R_{\text{hdaf}} = B \log_2 \left(1 + \gamma_{\text{hdaf}}\right) . \tag{22}$$

where P_{hd} represents the transmit power at V_1, and P_{hdrel} corresponds to the transmit power of the HD-DF UAV relay. The amplification factor β_h for HD-AF UAV relay scheme can be calculated as:

$$\beta_h = \sqrt{\frac{P_{\text{hdrel}}}{P_{\text{hd}} \mid \mathbf{h}_{\text{sr}} \mid^2 + \sigma^2}}. \tag{23}$$

Hence, the transmit power for HD UAV relay scheme is given by:

$$P_{\text{hd}} + P_{\text{hdrel}} = P_{\text{tot}} - P_{\text{relay}} - \frac{1}{2}P_s - P_d. \tag{24}$$

where P_{relay} is the hardware-dissipated power at UAV relay. The assumption is made that equal power is allocated to V_1 and ARIS or UAV relay to transmit the signals.

C. UAV ENERGY CONSUMPTION MODEL

The UAV energy consumption model used in this paper was adopted from [19], where the energy model considered 3D multi-rotor UAVs in three flight statuses, i.e., forward flight, vertical descent ascent, and vertical ascent. The UAV energy consumption model can be represented by the following equation:

$$\begin{aligned} rClE_{\text{flig}}(V_u) = {} & P_{\text{hov}} + \frac{3}{8}\sqrt{n}\delta\sqrt{\frac{W\rho A}{C_T}}s\|V_h\|^2 \\ & + P_{\text{in}}\left[\left(\sqrt{1 + \frac{\|V_h\|^4}{4v_0^4}} - \frac{\|V_h\|^2}{2v_0^2}\right)^{1/2} - 1\right] \\ & + \frac{n}{2}S_H\rho\|V_h\|^3 + \frac{1}{2}W\|V_v\| \\ & + \text{sign}(V_v)\frac{n}{4}S_V\rho\|V_v\|^3 \\ & + \left(\frac{W}{2} + \text{sign}(V_v)\frac{n}{4}S_V\rho\|V_v\|^2\right) \\ & \times\sqrt{\left(1 + \frac{\text{sign}(V_v)S_V}{A}\right)\|V_v\|^2 + \frac{2W}{n\rho A}} \\ & + (\text{sign}(\|V_v\|) - 1)\frac{W}{2}\sqrt{\frac{2W}{n\rho A}}. \end{aligned} \tag{25}$$

The variables P_{hov} and P_{in} represent the hover power and induced power of UAV, respectively. The induced power is calculated as:

$$P_{\text{in}} = (1 + k)\frac{W^{\frac{3}{2}}}{\sqrt{2n\rho A}}. \tag{26}$$

Thus, total flight consumption in equation (25) consists of three components which are hovering power, power consumption due to increment in the horizontal motion of ARIS with horizontal velocity, V_h and the power consumed during vertical ascent and descent with vertical velocity, V_v. In this paper, P_{hov} is omitted from the equation since

ARIS is moving all the time where ARIS velocity is not equal to zero. Considering the energy produced by ARIS flight (E_{flig}) is significantly more than the energy used by communication (E_{comm}), therefore, two weight factors α_1 and α_2 are introduced in the total energy consumption [20]. Consequently, ARIS weighted overall energy consumption and EE can be calculated as:

$$E = \alpha_1 E_{\text{comm}} + \alpha_2 E_{\text{flig}} \tag{27}$$

and

$$\text{EE} = R/E\ . \tag{28}$$

III. ENERGY EFFICIENCY OPTIMIZATION

In this paper, the 3D position and transmit power of the ARIS are jointly optimized to maximize the system's energy efficiency (EE), subject to a minimum rate requirement and a total power constraint. The corresponding optimization problem is formulated as:

$$P1: \max_{x_a, y_a, z_a, P} \frac{R}{E} \tag{29}$$

$$s.t.\ C1: Z_{\min} \le Z \le Z_{\max} \tag{29a}$$

$$C2: X_{\min} \le X \le X_{\max} \tag{29b}$$

$$C3: V_H \le V_{\text{Hmax}} \tag{29c}$$

$$C4: V_V \le V_{\text{Vmax}} \tag{29d}$$

$$C5: P_h + NP_{\text{sw}} + LP_{\text{dc}} + P_s + P_d \le P_{\max} \tag{29e}$$

$$C6: P_p + NP_{\text{sw}} + P_s + P_d \le P_{\max} \tag{29f}$$

$$\text{C7: } R \ge R_{\min}. \tag{29g}$$

Note that x_a, y_a, z_a and P denote the optimization parameters representing the 3D position and transmit power of ARIS, respectively, where $P = P_h + P_{\text{ris}}$ for hybrid ARIS, and $P = P_p$ for passive ARIS. $C1$ defines the constraint for minimum and maximum boundaries for flying ARIS. As stated in $C2$, $X_{\min}$ and $X_{\max}$ are the minimum and maximum values for ARIS's horizontal position in ARIS's coverage area while $C3$ and $C4$ are ARIS's velocity limit in horizontal and vertical directions, respectively. Constraints $C5$ and $C6$ is to ensure that hybrid ARIS's transmit power, P_h and passive ARIS's transmit power, P_p remain within the maximum allowable threshold power of $P_{\max}$, respectively. Instead of adopting specific QoS metrics as used in [21], we utilize a more general metric which is the minimum rate requirement, formulated as constraint $C7$. This constraint ensures that the system achieves at least the minimum data rate, $R_{\min}$, thereby fulfilling the QoS requirements of the communication link. Solving the optimization problem in (29) directly is difficult because of its fractional structure and the non-convex nature of the objective function.

A 3D plot is used to examine the relationship between the objective function and the optimization variables. Fig. 2 shows the 3D surface plot for hybrid ARIS. The 3D surface plot for hybrid ARIS scheme demonstrates the EE in bits/Joule as a function of both ARIS's vertical and horizontal position within the maximum transmit power. The plot indicates that there is an optimal operating region for maximizing EE of hybrid ARIS. The 3D surface plot shapes are identical for all powers within the range of study. Thus, for a given transmit power, the EE exhibits quasiconcavity with respect to the vertical and horizontal position of ARIS. This feature guarantees the local maximum

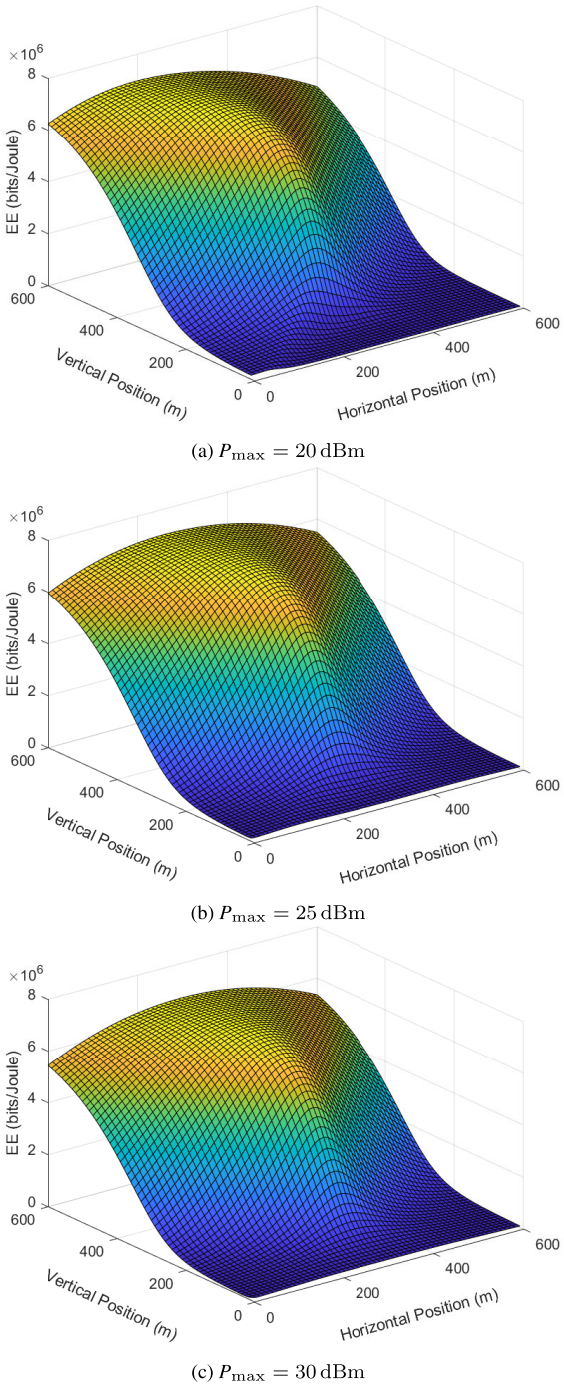

FIGURE 2. 3D surface plots for hybrid ARIS scheme at $P_{\max}$ values of 20 dBm, 25 dBm, and 30 dBm.

found from the optimization algorithm will also be a global maximum [22].

The 3D surface plot graph for passive ARIS is illustrated in Fig. 3. The EE equation is also appeared to be a quasiconcave function, with at least three optimum points within the observation time (one optimum point is global while another two are locals). Thus, in order for the algorithm to accurately finding the global optimum for each point of distance, we properly tuned the initial searching point paramaters in interior point method to exclude the local points so that global point could be found.

An efficient iterative algorithm for EE maximization, utilizing the Dinkelbach method [23] is proposed for addressing the equivalent problem (29), as detailed in Algorithm 1. It begins by initializing the transmit power and ARIS's 3D position and calculating the initial EE, q^1. During each iteration, the optimization problem is tackled using interior point method by maximizing the difference between the achievable rate and total power consumption, $R - q^k E$. Solving this subproblem yields updated power and 3D position values, which are used to compute a new EE. The iterations continue until the improvement becomes negligible which is less than the predefined threshold, ϵ and the maximum number of iterations is reached. This method is effective for fractional problems where this approach guarantees convergence to the optimal solution. The proof of convergence is omitted due to its similarity with the one in [23].

IV. NUMERICAL PERFORMANCE COMPARISON

This section analyzes the EE performance of ARIS-assisted V2V system. We use Monte Carlo simulations and parameter settings in Table 1 to evaluate system performance. The environment parameters are set based on urban area scenarios, where the effect of Doppler shift is negligible as vehicles are moving at lower speeds. We set the velocity for V_1 and V_2 at 12 ms^{-1} and 15 ms^{-1}, respectively. V_1, V_2, and UAV relay are each equipped with a single antenna. Consequently, the number of reflecting elements for passive ARIS is set to 256 in the default setup. The hybrid ARIS scheme is outfitted with only one active element.

In this section, we compare hybrid ARIS scheme with passive ARIS scheme and aerial relay. The following benchmark schemes are used for performance comparison:

- non-optimized hybrid ARIS and passive ARIS: In these schemes, the horizontal position of ARIS is fixed in the middle position between vehicles while the vertical position and power are fixed at 10 m and 30 dBm, respectively.
- half-duplex Amplify and Forward (AF) / Decode and Forward (DF) relay: Instead of employing ARIS, these schemes use UAV relay to reflect the signals. We utilize the same values for ARIS's positions and power with non-optimized hybrid ARIS scheme and passive ARIS to ensure a fair comparison.

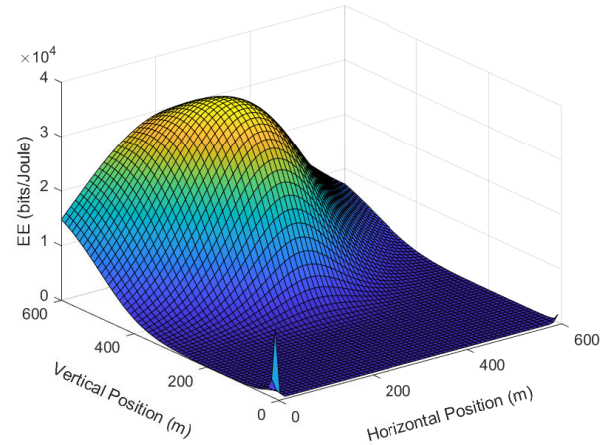

(a) $P_{\max} = 20\,\text{dBm}$

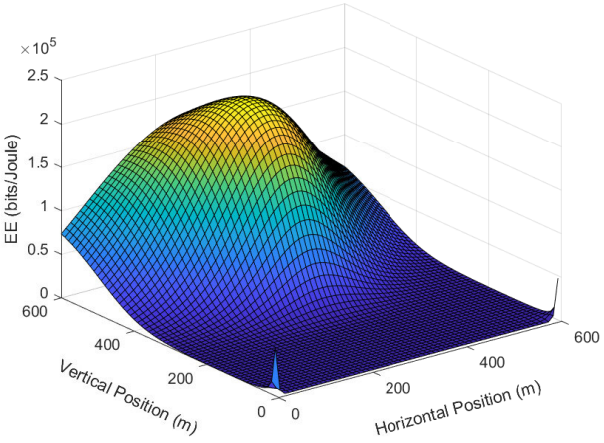

(b) $P_{\max} = 25\,\text{dBm}$

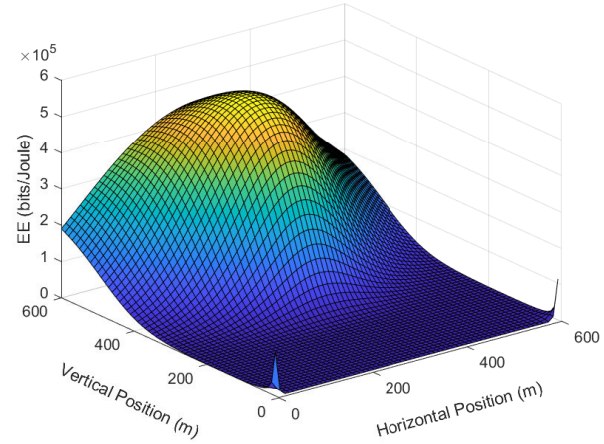

(c) $P_{\max} = 30\,\text{dBm}$

FIGURE 3. 3D surface plots for passive ARIS scheme at $P_{\max}$ values of 20 dBm, 25 dBm, and 30 dBm.

A. ENERGY EFFICIENCY

Fig. 4 illustrates the energy efficiency (in Mbits/Joule) as a function of the relative distance between V_1 and V_2, comparing different schemes at two operating frequencies: 2.3 GHz and 5.9 GHz. For all schemes, EE decreases as

Algorithm 1 EE Maximization Optimization Algorithm for Jointly Optimized Transmit Power and ARIS 3D Position

Initialization

Set iteration index $k = 1$ and maximum iteration count $L_{\max} = 100$.

Set convergent threshold $\epsilon = 0.00001$.

Choose an initial point $(P^{(1)}, x_a^{(1)}, z_a^{(1)})$ within feasible bounds.

Compute initial EE:

$$q^{(1)} = \frac{R(P^{(1)}, x_a^{(1)}, z_a^{(1)})}{E(P^{(1)}, x_a^{(1)}, z_a^{(1)})}$$

Iterative Algorithm

repeat

Solve the auxiliary problem using interior point method:

$$(P^{(k)}, x_a^{(k)}, z_a^{(k)}) = \max_{P, x_a, z_a} \left[R(P, x_a, z_a) - q^{(k)} E(P, x_a, z_a) \right]$$

Update EE:

$$q^{(k+1)} = \frac{R(P^{(k)}, x_a^{(k)}, z_a^{(k)})}{E(P^{(k)}, x_a^{(k)}, z_a^{(k)})}$$

if $R(P^{(k)}, x_a^{(k)}, z_a^{(k)}) - q^{(k)} E(P^{(k)}, x_a^{(k)}, z_a^{(k)}) < \epsilon$ **then**

Stop and return $(P^*, x_a^*, z_a^*) = (P^{(k)}, x_a^{(k)}, z_a^{(k)}), q^* = q^{(k)}$

else $k \leftarrow k + 1$

end if

until convergence and $k = L_{\max}$

Output: Optimal 3D ARIS position and transmit power (P^*, x_a^*, z_a^*), and optimal EE q^*

TABLE 1. Simulation parameters.

Notation	Physical meaning	Value
α_1	Weight factor for communication power	1
α_3	Weight factor for UAV power	0.01
P_{tot}	Total communication power	30 dBm
v_0	Mean rotor induced velocity in hover	6.325 ms^{-1}
ρ	Air density	1.168 kgm^{-3}
s	Rotor solidarity	0.045
A	Rotor disc area	0.214 m^2
n	Number of rotor	4
δ	Profile drag coefficient	0.011
W	UAV weight in Newton	20
C_T	Coefficient of thrust	0.001195
S_H	Horizontal fuselage	0.009 m^2
S_V	Vertical fuselage	0.377 m^2
k	Incremental correction factor to induced power	0.11
α_e	LoS constant value	1.5
α_0	NLoS constant value	2
a	Environmental parameters constant	11.95
b	Environmental parameters constant	0.136
$K_{\min}$	minimum Rician factor	5 dB
$K_{\max}$	maximum Rician factor	15 dB
f_c	operating frequency	2.3 GHz
B	System bandwidth	10 MHz
σ_r^2, σ^2	Noise power	-90 dBm
P_{sw}	Power consumption of phase shift switches and control circuits at each RIS element	-10 dBm
P_s, P_d	Hardware dissipation power at vehicles	10 dBm
N	Number of RIS elements	256
$X_{\min}$	minimum ARIS horizontal value	0
$X_{\max}$	maximum ARIS horizontal value	600 m
$Z_{\min}$	minimum ARIS vertical value	10 m
$Z_{\max}$	maximum ARIS vertical value	100 m
V_{Hmax}	maximum ARIS horizontal velocity	15 ms^{-1}
V_{Vmax}	maximum ARIS vertical velocity	6 ms^{-1}
$P_{\min}$	minimum power transmit value	0.1 W
$P_{\max}$	maximum power transmit value	1 W
$R_{\min}$	minimum rate requirement	5 MHz [24]
L_b	number of bits per packet	1024

the distance between the vehicles increases. In general, hybrid ARIS scheme outperforms passive ARIS and aerial relay schemes. The slower decline in EE observed in hybrid ARIS compared to passive ARIS suggests that the benefits of signal amplification are sustained over longer distances. The proposed hybrid ARIS, optimized with the proposed algorithm, shows the highest EE across all distances, where the algorithm effectively optimized the transmit power and ARIS's 3D positions to achieve the best overall EE. Despite having an intermediate performance, the non-optimized hybrid ARIS scheme still outperforms passive ARIS, as it can amplify signals with only a single active element, thereby enhancing EE. While the proposed optimization improves the EE of passive ARIS scheme, it remains less efficient compared to the proposed optimized hybrid ARIS scheme, as it relies solely on passive elements and is affected by the double path loss [11]. Furthermore, the EE of passive ARIS degrade significantly with increasing distance, whereas the aerial relay scheme maintains better EE over longer distances, due to its built-in amplifier. Additionally, using fixed power and fixed UAV position in the half-duplex relay configurations results in consistently low EE, which proves the benefit of the proposed technique. The combination of the precise placement of ARIS and optimal transmit power leads to superior performance of the proposed hybrid ARIS. This is evident from its higher EE values and more gradual decline with distance in the graph. Furthermore, it can be observed that operating at a higher frequency (5.9 GHz) incurs more severe path loss, thereby reducing the overall EE compared to operation at a lower frequency (2.3 GHz).

Fig. 5 presents the EE for all considered schemes as a function of the number of passive and active elements. For all schemes, especially passive ARIS, the EE improves as the total number of elements increases. It is observed that schemes with 256 elements ($N = 256$) yield higher EE than those with 64 elements ($N = 64$). Furthermore, the inclusion of active elements in hybrid ARIS offers the best performance in EE due to its ability to amplify signals. An increase in the number of active elements (e.g., when L increases from 1 to 3) leads to a further enhancement in the EE performance of hybrid ARIS. The proposed hybrid ARIS, optimized with the proposed algorithm, demonstrates superior EE compared to passive ARIS scheme. Even with

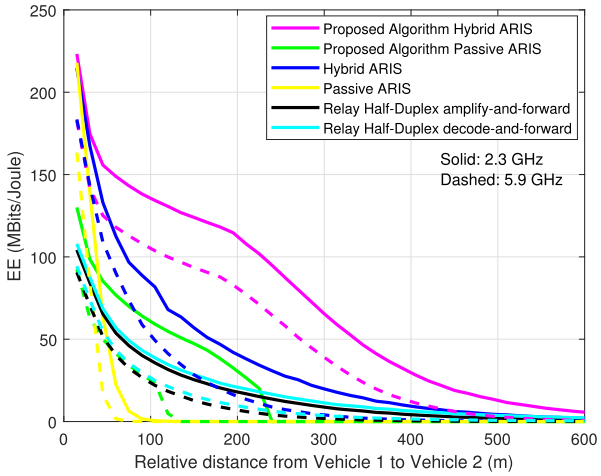

FIGURE 4. Energy efficiency (EE) comparison of all considered schemes at 2.3 GHz and 5.9 GHz.

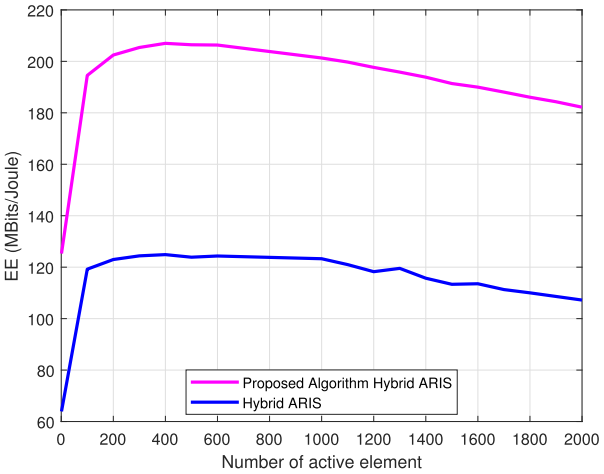

FIGURE 6. EE of hybrid ARIS versus number of active elements.

just a single active element (i.e., $L = 1$), hybrid ARIS achieves a remarkable improvement in EE, striking a balance between performance enhancement and the combined energy and hardware costs. Although both hybrid ARIS and aerial relay schemes employ amplification, hybrid ARIS achieves higher EE due to its lower power requirements. In contrast, the aerial relay relies on large power budget, resulting in increased energy consumption [11].

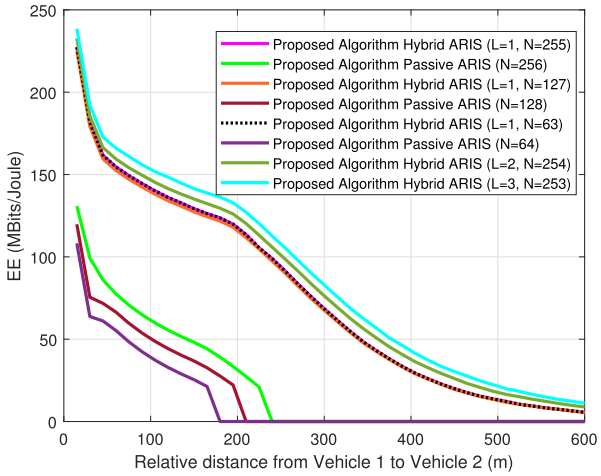

FIGURE 5. EE performance with different numbers of passive and active elements.

Fig. 6 illustrates the EE performance of the proposed algorithm compared to baseline hybrid ARIS schemes with an increasing number of active elements. For both schemes, the EE initially increases due to enhanced signal amplification; however, beyond approximately 400 active elements, the power consumption of active components begins to dominate, causing the EE to decline. This degradation occurs due to the rising power consumption associated with the additional active hardware, which outweighs the performance gains. The proposed algorithm outperforms the baseline scheme, highlighting its capability to optimally balance the trade-off between signal rate and power consumption through joint optimization of transmit power and ARIS 3D position. These results validate the effectiveness of the proposed method in improving the EE of ARIS-assisted communication.

The effect of imperfect channel state information (CSI) under varying levels of statistical CSI error on EE is illustrated in Fig. 7. In this work, statistical CSI error is considered, where the CSI estimation error is random and follows a specific distribution [25], [26]. The estimated channels are denoted by $\hat{\mathbf{h}}_{\text{sr}}$ and $\hat{\mathbf{h}}_{\text{rd}}$, while $\Delta\mathbf{h}_{\text{sr}}$ and $\Delta\mathbf{h}_{\text{rd}}$ represent the corresponding channel estimation errors. The imperfect CSI model is expressed as $\mathbf{h}_{\text{sr}} = \hat{\mathbf{h}}_{\text{sr}} + \Delta\mathbf{h}_{\text{sr}}$ and $\mathbf{h}_{\text{rd}} = \hat{\mathbf{h}}_{\text{rd}} + \Delta\mathbf{h}_{\text{rd}}$ where $\Delta\mathbf{h}_{\text{sr}} \sim \mathcal{CN}(0, \sigma_{e_1}^2)$ and $\Delta\mathbf{h}_{\text{rd}} \sim \mathcal{CN}(0, \sigma_{e_2}^2)$ represent the channel estimation error for each channel which follows the complex Gaussian distribution with mean 0 and with variances $\sigma_{e_1}^2$ and $\sigma_{e_2}^2$, respectively.

Under perfect CSI, the proposed hybrid ARIS scheme achieves the highest EE performance compared to passive ARIS. However, when CSI imperfection is introduced, the EE performance of both schemes degrades. The performance degradation is small for $\sigma_{e_1} = \sigma_{e_2} = 0.01$, which represents the typical channel estimation error variance [27], [28] of minimum mean square error (MMSE) scheme at high SNR. However, for $\sigma_{e_1} = \sigma_{e_2} = 0.1$, which represents the typical channel estimation error variance of MMSE scheme at low SNR, the EE decreases further due to more severe channel estimation error. The result confirms that the proposed hybrid ARIS scheme demonstrates robustness against CSI inaccuracies, and it can maintain superior EE performance compared to passive ARIS scheme even in the presence of CSI errors.

B. TRAJECTORY

The graph in Fig. 8 shows the optimized trajectories selected by hybrid and passive ARIS schemes, based on their respective amplification capabilities and system constraints.

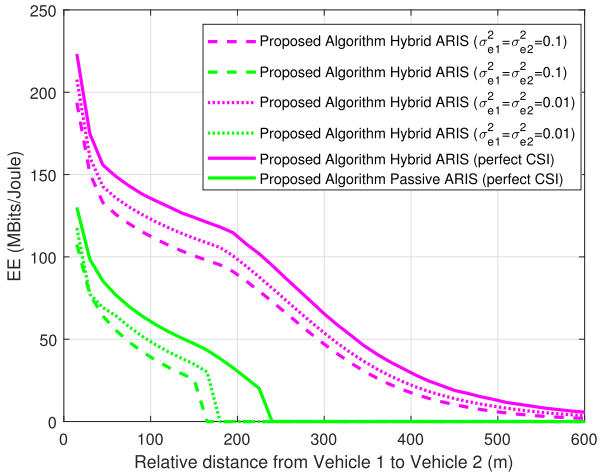

FIGURE 7. EE comparison under imperfect channel state information (CSI).

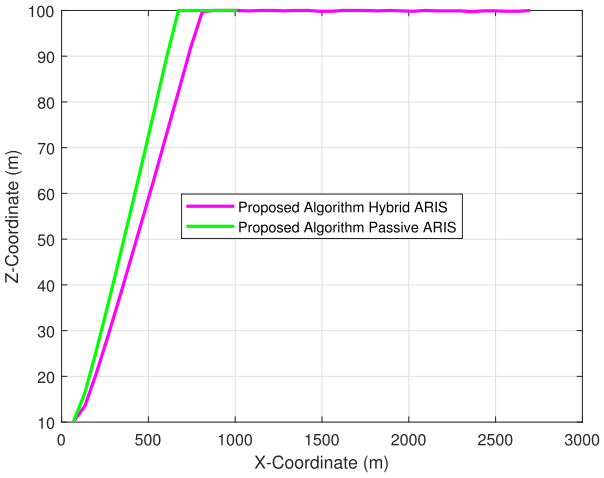

FIGURE 8. Trajectory of hybrid and passive ARIS.

The trajectory for hybrid ARIS starts at a low altitude and increases, showing a smooth ascent until around 800 m of x-coordinate, then levels off around 100 m of z-coordinate. The hybrid ARIS scheme chooses to fly towards the middle position between V_1 and V_2 and higher up to 100 m of altitude to get better LoS and improved communication links. The hybrid ARIS algorithm suggests a more extensive optimization process in both vertical and horizontal dimensions, contributing to its superior EE performance. The trajectory for optimized passive ARIS has a steeper initial slope and stabilizes at the x-coordinates of 700 m earlier than hybrid ARIS, then hovers at the same position. Since passive ARIS relies solely on signal reflection without amplification, the SNR drops to zero, causing ARIS to hover at the same position after reaching its maximum altitude. Fig. 8 validates the effectiveness of the proposed algorithms, which adapt the trajectory based on the specific capabilities of each scheme.

C. POWER

Fig. 9 evaluates the efficiency of power allocation strategies based on the proposed algorithms as a function of the relative distance from V_1 to V_2. The proposed hybrid ARIS, optimized with the proposed algorithm, shows a gradual increase in power, suggesting that the proposed algorithm optimizes power usage dynamically. The scheme increases the power as the distance increases to maintain its EE and signal quality. This dynamic adjustment contributes to its higher EE. In contrast, the transmit power for passive ARIS scheme remains constant at the maximum power limit (30 dBm) across all distances. This behavior is due to the limited capability of passive surfaces to compensate for signal attenuation; as the path loss increases with distance, the passive ARIS requires maximum allowable transmit power to satisfy the minimum rate constraints. The ability to adapt power requirements more precisely due to the existence of an active element is the main reason why the proposed hybrid ARIS scheme achieves better overall performance compared to passive ARIS.

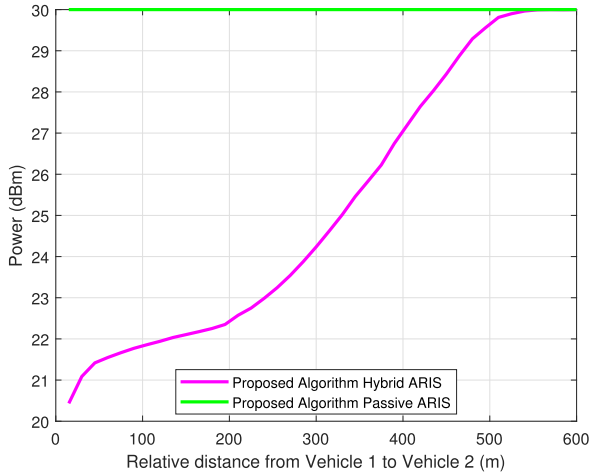

FIGURE 9. Transmit power versus relative distance between V_1 and V_2.

D. VELOCITY

Fig. 10 illustrates the mobility behavior of both hybrid and passive ARIS schemes according to the proposed optimization algorithms. It presents the vertical and horizontal velocities of each ARIS type as a function of the relative distance between V_1 and V_2, providing insight into their dynamic movement strategies. Four different profiles are illustrated in the graph. The dashed lines represent the horizontal velocities, while the solid lines are the vertical velocities of both hybrid and passive ARIS, respectively. The horizontal velocity for hybrid ARIS is relatively constant and low throughout the entire distance range, which indicates a stable horizontal movement without significant changes. In contrast, for passive ARIS, the horizontal velocity starts low but increases significantly as the distance increases.

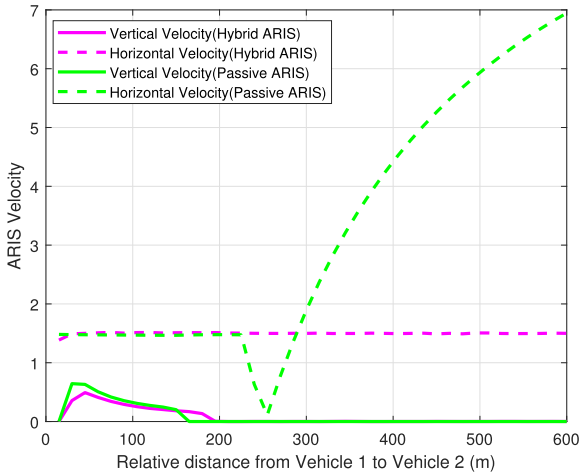

FIGURE 10. Vertical and horizontal ARIS velocity versus relative distance between V_1 and V_2.

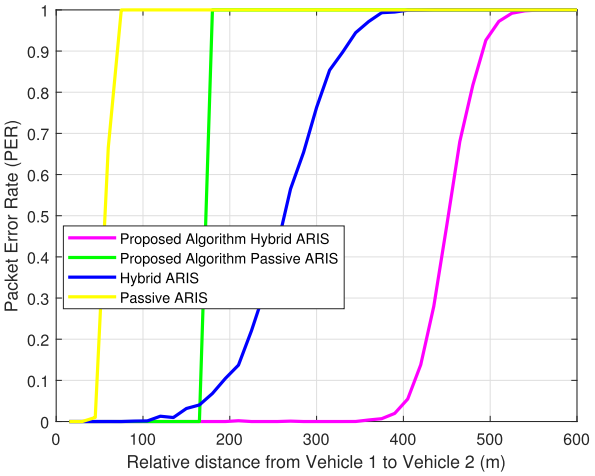

FIGURE 11. Packet error rate (PER) versus relative distance between V_1 and V_2.

Hybrid ARIS does not need to rely as heavily on physical repositioning to maintain effective communication, as it can actively boost and manipulate signals. It can enhance the signal strength and quality even when movement is minimized. Thus, it can use its energy reserves more for active signal manipulation rather than for frequent, rapid movements. The sharp peaks in passive ARIS system's horizontal velocities indicate the need for further tuning to increase the signal reflection. As passive ARIS relies solely on the physical adjustment of its reflective surface to optimize the signal, it must align effectively and continually reposition itself with the changing positions of the vehicles it serves. On the other hand, the vertical velocities for both hybrid and passive ARIS start low and stay relatively constant, showing minor fluctuations and stabilizes to a low value. Both schemes maintain low vertical velocities to obtain better EE. The differences in passive and hybrid operational highlights how each system's capabilities influence their mobility strategies and EE in practical scenarios.

E. PACKET ERROR RATE

Fig. 11 illustrates the packet error rate (PER) of the proposed algorithms as a function of the relative distance between vehicles. PER serves as an important indicator of assessing transmission reliability [29], where maintaining a low PER is essential for achieving reliable throughput. In general, the reliability of data transmission is evaluated using two key performance metrics: the bit error rate (BER) and the PER. Assuming binary phase-shift keying (BPSK) as the modulation scheme, the BER and PER are evaluated as [29]:

$$\text{BER} = Q\left(\sqrt{2\gamma}\right) \tag{30}$$

and

$$\text{PER} = 1 - (1 - \text{BER})^{L_b}. \tag{31}$$

where L_b is the number of bits per packet, and Q represents the tail probability of the standard normal distribution.

As observed in Fig. 11, the proposed algorithm improves both passive and hybrid ARIS systems. The proposed optimized hybrid ARIS scheme outperforms the others by maintaining a near-zero PER up to approximately 400 m. Similarly, the proposed passive ARIS demonstrates improved reliability, achieving error-free communication up to 170 m. In contrast, conventional passive ARIS experiences a rapid increase in PER beyond 50 m, indicating limited communication reliability. Although the conventional hybrid ARIS shows improvement over optimized passive ARIS, its PER remains higher than that of the proposed optimized hybrid ARIS, primarily due to the absence of algorithmic robustness. These results highlight the effectiveness of the proposed algorithm in enhancing communication reliability over extended V2V distances.

V. CONCLUSION

In this paper, we proposed a hybrid ARIS-assisted V2V communication scheme to enhance the EE of the communication system. We compare hybrid ARIS with passive ARIS scheme and aerial relay schemes. Through numerical simulations, it is clear that hybrid ARIS with optimized 3D position and transmit power delivers unparalleled benefits when compared to passive ARIS, and other benchmark systems in terms of EE. The active element in hybrid ARIS extends V2V communication by amplifying signals over longer distances within lower power budget ensuring reliable connectivity. Even with just one active element, it outperforms other schemes in terms of EE. This emphasize the significant roles of optimized hybrid ARIS in enhancing the performance of V2V communication networks.

ACKNOWLEDGMENT

Norlezah Hashim would like to thank the Ministry of Higher Education Malaysia and Universiti Teknikal Malaysia Melaka for the scholarships.

An earlier version of this paper was presented in part at the IEEE 16th Malaysia International Conference on Communication [DOI: 10.1109/MICC59384.2023.10419824].

REFERENCES

[1] M. U. Sheikh, J. Hämäläinen, G. D. Gonzalez, R. Jäntti, and O. Gonsa, "Usability benefits and challenges in mmWave V2V communications: A case study," in *Proc. Int. Conf. Wireless Mobile Comput., Netw. Commun. (WiMob)*, Barcelona, Spain, Oct. 2019, pp. 1–5, doi: 10.1109/WiMOB.2019.8923432.

[2] S. Wahb, E. A. Maher, and A. El-Mahdy, "Reflecting intelligent surface assisted vehicular communication networks," in *Proc. 4th Novel Intell. Lead. Emerg. Sci. Conf. (NILES)*, Giza, Egypt, Oct. 2022, pp. 190–193, doi: 10.1109/NILES56402.2022.9942429.

[3] Y. Chen, Y. Wang, J. Zhang, P. Zhang, and L. Hanzo, "Reconfigurable intelligent surface (RIS)-aided vehicular networks: Their protocols, resource allocation, and performance," *IEEE Veh. Technol. Mag.*, vol. 17, no. 2, pp. 26–36, Jun. 2022, doi: 10.1109/MVT.2022.3158046.

[4] B. M. Masini, C. M. Silva, and A. Balador, "The use of meta-surfaces in vehicular networks," *J. Sensor Actuator Netw.*, vol. 9, no. 1, p. 15, Mar. 2020, doi: 10.3390/jsan9010015.

[5] P. Saikia, S. Pala, K. Singh, S. K. Singh, and W.-J. Huang, "Proximal policy optimization for RIS-assisted full duplex 6G-V2X communications," *IEEE Trans. Intell. Vehicles*, vol. 9, no. 7, pp. 5134–5149, Jul. 2024, doi: 10.1109/TIV.2023.3275632.

[6] Y. U. Ozcan, O. Ozdemir, and G. K. Kurt, "Reconfigurable intelligent surfaces for the connectivity of autonomous vehicles," *IEEE Trans. Veh. Technol.*, vol. 70, no. 3, pp. 2508–2513, Mar. 2021, doi: 10.1109/TVT.2021.3060667.

[7] Y. Cao, S. Xu, J. Liu, and N. Kato, "Toward smart and secure V2X communication in 5G and beyond: A UAV-enabled aerial intelligent reflecting surface solution," *IEEE Veh. Technol. Mag.*, vol. 17, no. 1, pp. 66–73, Mar. 2022, doi: 10.1109/MVT.2021.3136832.

[8] M. Eskandari, H. Huang, A. V. Savkin, and W. Ni, "Model predictive control-based 3D navigation of a RIS-equipped UAV for LoS wireless communication with a ground intelligent vehicle," *IEEE Trans. Intell. Vehicles*, vol. 8, no. 3, pp. 2371–2384, Mar. 2023, doi: 10.1109/TIV.2022.3232890.

[9] M. Eskandari, A. V. Savkin, and W. Ni, "Consensus-based autonomous navigation of a team of RIS-equipped UAVs for LoS wireless communication with mobile nodes in high-density areas," *IEEE Trans. Autom. Sci. Eng.*, vol. 20, no. 2, pp. 923–935, Apr. 2023, doi: 10.1109/TASE.2022.3183335.

[10] N. Hashim, C. Y. Leow, C. H. Foh, S. K. A. Rahim, and J. Jayakumari, "Aerial reconfigurable intelligent surface for vehicle-to-vehicle communication," in *Proc. IEEE 16th Malaysia Int. Conf. Commun. (MICC)*, Kuala Lumpur, Malaysia, Dec. 2023, pp. 86–90, doi: 10.1109/MICC59384.2023.10419824.

[11] C. Y. Goh, C. Y. Leow, and R. Nordin, "Energy efficiency of unmanned aerial vehicle with reconfigurable intelligent surfaces: A comparative study," *Drones*, vol. 7, no. 2, p. 98, Jan. 2023, doi: 10.3390/drones7020098.

[12] N. T. Nguyen, Q.-D. Vu, K. Lee, and M. Juntti, "Hybrid relay-reflecting intelligent surface-assisted wireless communications," *IEEE Trans. Veh. Technol.*, vol. 71, no. 6, pp. 6228–6244, Jun. 2022, doi: 10.1109/TVT.2022.3158686.

[13] M. Matracia, M. A. Kishk, and M.-S. Alouini, "Comparing aerial-RIS- and aerial-base-station-aided post-disaster cellular networks," *IEEE Open J. Veh. Technol.*, vol. 4, pp. 782–795, 2023, doi: 10.1109/OJVT.2023.3316117.

[14] L. Ge, H. Zhang, and J. Wang, "Joint placement and beamforming design in multi-UAV-IRS assisted multiuser communication," in *Proc. IEEE Global Commun. Conf. (GLOBECOM)*, Madrid, Spain, Dec. 2021, pp. 01–06, doi: 10.1109/GLOBECOM46510.2021.9685505.

[15] M. M. Azari, F. Rosas, K.-C. Chen, and S. Pollin, "Ultra reliable UAV communication using altitude and cooperation diversity," *IEEE Trans. Commun.*, vol. 66, no. 1, pp. 330–344, Jan. 2018, doi: 10.1109/TCOMM.2017.2746105.

[16] A. Al-Hourani, S. Kandeepan, and S. Lardner, "Optimal LAP altitude for maximum coverage," *IEEE Wireless Commun. Lett.*, vol. 3, no. 6, pp. 569–572, Dec. 2014, doi: 10.1109/LWC.2014.2342736.

[17] K. Zhi, C. Pan, H. Ren, K. K. Chai, and M. Elkashlan, "Active RIS versus passive RIS: Which is superior with the same power budget?" *IEEE Commun. Lett.*, vol. 26, no. 5, pp. 1150–1154, May 2022, doi: 10.1109/LCOMM.2022.3159525.

[18] E. Björnson, Ö. Özdogan, and E. G. Larsson, "Intelligent reflecting surface versus decode-and-forward: How large surfaces are needed to beat relaying?" *IEEE Wireless Commun. Lett.*, vol. 9, no. 2, pp. 244–248, Feb. 2020, doi: 10.1109/LWC.2019.2950624.

[19] H. Gong, B. Huang, B. Jia, and H. Dai, "Modeling power consumptions for multirotor UAVs," *IEEE Trans. Aerosp. Electron. Syst.*, vol. 59, no. 6, pp. 7409–7422, Dec. 2023, doi: 10.1109/TAES.2023.3288846.

[20] J. Chen, Y. Xu, D. Yang, and T. Zhang, "UAV-assisted ISCC networks: Joint resource and trajectory optimization," *IEEE Wireless Commun. Lett.*, vol. 13, no. 9, pp. 2372–2376, Sep. 2024, doi: 10.1109/LWC.2024.3415084.

[21] M. A. Saleem, S. Zhou, Z. Fengli, T. Ahmad, N. Nigar, M. U. Hadi, and M. Shabaz, "Delay, energy, and outage considerations in GenAI-enhanced MEC-NOMA-enabled vehicular networks," *IEEE Trans. Intell. Transp. Syst.*, early access, Mar. 18, 2025, doi: 10.1109/TITS.2025.3548268.

[22] F. Idris, J. Tangm, and D. K. C. So, "Resource and energy efficient device-to-device communications in downlink cellular system," in *Proc. IEEE Wireless Commun. Netw. Conf. (WCNC)*, Barcelona, Spain, Apr. 2018, pp. 1–6, doi: 10.1109/WCNC.2018.8377382.

[23] W. Dinkelbach, "On nonlinear fractional programming," *Manage. Sci.*, vol. 13, no. 7, pp. 492–498, Mar. 1967, doi: 10.1287/mnsc.13.7.492.

[24] S. Maurya, R. Gour, S. Yadav, S. Singh, and M. Bansal, "Outage analysis of two-way full-duplex RIS-assisted V2V networks with user selection," in *Proc. IEEE 8th Int. Conf. Inf. Commun. Technol. (CICT)*, Prayagraj, India, Dec. 2024, pp. 1–5, doi: 10.1109/CICT64037.2024.10899451.

[25] Z. Peng, Z. Chen, C. Pan, G. Zhou, and H. Ren, "Robust transmission design for RIS-aided communications with both transceiver hardware impairments and imperfect CSI," *IEEE Wireless Commun. Lett.*, vol. 11, no. 3, pp. 528–532, Mar. 2022, doi: 10.1109/LWC.2021.3135413.

[26] K. M. Hamza, S. Basharat, S. A. Hassan, and H. Jung, "On the secrecy performance of RIS-enhanced aerial communication under imperfect CSI," in *Proc. IEEE Conf. Comput. Commun. Workshops (INFOCOM WKSHPS)*, Hoboken, NJ, USA, May 2023, pp. 1–6, doi: 10.1109/INFOCOMWKSHPS57453.2023.10226064.

[27] F. A. P. de Figueiredo, F. A. C. M. Cardoso, I. Moerman, and G. Fraidenraich, "Channel estimation for massive MIMO TDD systems assuming pilot contamination and flat fading," *EURASIP J. Wireless Commun. Netw.*, vol. 2018, no. 1, Jan. 2018, Art. no. 14, doi: 10.1186/s13638-018-1021-9.

[28] M. Hayajneh and T. A. Gulliver, "Physical layer security in two-way SWIPT relay networks with imperfect CSI and a friendly jammer," *Entropy*, vol. 25, no. 1, p. 122, Jan. 2023, doi: 10.3390/e25010122.

[29] A. Goldsmith, *Wireless Communications*. Cambridge, U.K.: Cambridge Univ. Press, 2005.

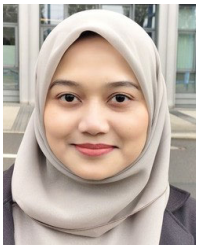

NORLEZAH HASHIM (Graduate Student Member, IEEE) received the bachelor's degree in telecommunication engineering from University of Malaya, in 2006, and the master's degree in electrical and electronics engineering from University Teknologi Malaysia, Malaysia, in 2014, where she is currently pursuing the Ph.D. degree in electrical engineering under wireless communication center. Her current research interests include reconfigurable intelligent surface (RIS), unmanned aerial vehicle (UAV), vehicle-to-vehicle (V2V) communications, optimization in wireless communications, and non-orthogonal multiple access (NOMA).

CHEE YEN (BRUCE) LEOW (Senior Member, IEEE) received the B.Eng. degree in computer engineering from Universiti Teknologi Malaysia (UTM), in June 2007, and the Ph.D. degree in wireless communications from the Imperial College London, in September 2011.

He is currently an Associate Professor with the Faculty of Electrical Engineering and a Research Fellow with the Wireless Communication Centre, UTM. He is also a Secretary with the IMT and Future Networks Working Group under the Malaysian Technical Standards Forum Berhad to accelerate the adoption of 5G IMT-2020 in Malaysia. In addition, he regularly conducts short courses on 5G and IoT for the telecommunication industry. His current research interests include non-orthogonal multiple access, drone communications, intelligent surfaces, advanced MIMO, millimeter wave communications, prototype development using software-defined radio for beyond 5G, and the Internet of Things applications.

Dr. Leow's IEEE papers won the IEEE Malaysia Comsoc/VTS Joint Chapter's Best Paper Awards, in 2016, 2017, 2021, and 2022, and the IEEE Malaysia AP/MTT/EMC Joint Chapter's Best Paper Awards, in 2017, 2018, 2021, 2022, and 2024. He is chairing the IEEE Malaysia Comsoc/VTS Joint Chapter. He is a registered Chartered Engineer (CEng) of the Engineering Council, U.K., and a Professional Technologist of the Malaysia Board of Technologists. He is recognized as the Exemplary Editor of IEEE Wireless Communications Letters, in 2025.

KLAUS MOESSNER (Senior Member, IEEE) is currently a Professor of communications engineering with the University of Technology Chemnitz and a Professor of cognitive networks with the Institute for Communication Systems and the 5G Innovation Centre, University of Surrey. He was involved in many cognitive communications, service provision, and the IoT projects. He was responsible for the work on cognitive decision-making mechanisms in the CR Project ORACLE. He led the work on radio awareness in the ICT FP7 Project QoSMOS and led the H2020 Speed5G Project. He leads the EU-Taiwan Project Clear5G, investigating the extensions of 5G systems needed to serve the particular requirements of future factories. His research interests include cognitive networks, the IoT deployments, sensor data-based knowledge generation, reconfiguration, and resource management. He was the Founding Chair of the IEEE DYSPAN Working Group (WG6) on Sensing Interfaces for Future and Cognitive Communication Systems.

CHUAN HENG FOH (Senior Member, IEEE) received the M.Sc. degree from Monash University, Melbourne, VIC, Australia, in 1999, and the Ph.D. degree from the University of Melbourne, Melbourne, in 2002. After the Ph.D. degree, he spent six months as a Lecturer with Monash University. In December 2002, he joined Nanyang Technological University, Singapore, as an Assistant Professor, until 2012. He is currently an Associate Professor with the University of Surrey, Guildford, U.K. He has authored or co-authored more than 180 refereed papers in international journals and conferences. His research interests include protocol design, machine learning application, and performance analysis of various computer networks, including wireless local area networks, mobile ad-hoc and sensor networks, vehicular networks, the Internet of Things, 5G/6G networks, and open RAN. He served as the Vice Chair (Europe/Africa) for IEEE TCGCC, in 2015 and 2017. He is the Vice-Chair of the IEEE VTS Ad Hoc Committee on Mission Critical Communications. He is on the editorial boards of several international journals and a Senior Editor for IEEE Access.